communications earth & environment

ARTICLE

https://doi.org/10.1038/s43247-021-00299-0 OPEN

Projected increases in western US forest fire despite growing fuel constraints

John T. Abatzoglou[1✉], David S. Battisti[2], A. Park Williams[3,4], Winslow D. Hansen[5], Brian J. Harvey[6] & Crystal A. Kolden[1]

Escalating burned area in western US forests punctuated by the 2020 fire season has heightened the need to explore near-term macroscale forest-fire area trajectories. As fires remove fuels for subsequent fires, feedbacks may impose constraints on the otherwise climate-driven trend of increasing forest-fire area. Here, we test how fire-fuel feedbacks moderate near-term (2021–2050) climate-driven increases in forest-fire area across the western US. Assuming constant fuels, climate–fire models project a doubling of forest-fire area compared to 1991–2020. Fire-fuel feedbacks only modestly attenuate the projected increase in forest-fire area. Even models with strong feedbacks project increasing interannual variability in forest-fire area and more than a two-fold increase in the likelihood of years exceeding the 2020 fire season. Fuel limitations from fire-fuel feedbacks are unlikely to strongly constrain the profound climate-driven broad-scale increases in forest-fire area by the mid-21st century, highlighting the need for proactive adaptation to increased western US forest-fire impacts.

[1] Management of Complex Systems, University of California, Merced, CA, USA. [2] Department of Atmospheric Sciences, University of Washington, Seattle, WA, USA. [3] Department of Geography, University of California, Los Angeles, Los Angeles, CA, USA. [4] Lamont-Doherty Earth Observatory, Columbia University, Palisades, NY 10964, USA. [5] Cary Institute of Ecosystem Studies, Millbrook, NY, USA. [6] School of Environment and Forest Sciences, University of Washington, Seattle, WA, USA. ✉email: jabatzoglou@ucmerced.edu

The annual area burned by forest fires in the western United States (US) has increased ten-fold over the past half-century[1], punctuated by the record 2020 western US fire season that produced widespread negative effects[2]. Several anthropogenic factors underpin growing wildland fire area, including historically high fuel loads due to a century of fire suppression and outlawing of Indigenous burning; less direct suppression tactics to support firefighter safety, and increased fuel aridity due to human-caused climate change[3–6]. While the influence of these factors varies geographically as a function of both biophysical and human–environment interactions, climate variability expressed through fuel dryness is the dominant interannual driver of macroscale burned area across fuel-rich biomes in the western US and globe[7].

Increasing fuel aridity (F) and fire-weather extremes with continued climate change portend increased wildland fire activity where biomass is abundant and flammability is a primary constraint[8,9], including in western US forests[1,3]. Warming directly enhances fuel aridity by increasing the vapor pressure deficit (VPD) as well as reducing snowpack in montane regions, which collectively intensify and lengthen the fire season. Decreased summer precipitation in parts of the western US in recent decades has further increased fire-season F[10]. Most climate projections show increased F across the western US[11,12] and longer fire-weather seasons[13] that facilitate increased occurrence of fire-weather extremes in the autumn in California[14].

One key limitation in projecting trajectories of future fire is the degree to which decreasing available fuel will limit fire growth, suggesting eventual nonlinearities in contemporary climate–fire relationships[15,16]. Statistical models where climate alone drives changes in the burned area suggest massive future increases[17]. Such models assume sufficient fuels remain to support future burning, but there is strong evidence that increased forest-fire area may initiate fire-fuel feedbacks that limit future burned area[18] through the reduction of fuel biomass and extent, the ability of forested environments to carry fire[15], and the alteration of post-fire-vegetation patterns and climate that may limit tree regeneration[19]. Herein, we track fire-fuel feedbacks through a term called L, which represents the fraction of contemporary forested land that is incapable of carrying forest fire in a given year because it has been modified by fire in the recent past (~30 years) or through semi-permanent loss of forest due to post-fire tree regeneration failure. Recently burned areas can sometimes reburn at much shorter timescales—particularly with low-severity fire[20], in which case L will be less than the fraction of recently burned area. Fire can also create forest mosaics with reduced connectivity that are less prone to fire, in which case L exceeds the fraction of recently burned area. Studies have shown that fire-fuel feedbacks can moderate future changes in the burned area at local scales[21]. However, studies have not evaluated how fire-fuel feedbacks and climate will affect future fire activity at the scale of the entire western US forest area or the sensitivity of these projections to uncertainties in the duration and strength of the fire-fuel feedbacks.

Here, we use several possible forms of dynamic models that account for various fire-fuel feedbacks, a static model that does not incorporate vegetation feedbacks and assumes constant fuel extent, and projections of future climate change to bracket projected changes in near-term (2021–2050) western US forest-fire area. We additionally evaluate projected changes in the interannual variability of forest-fire area, the likelihood of years with a forest-fire area exceeding that observed in the record-breaking 2020 fire season, as well as the likelihood of years with a forest-fire area below the 1991–2020 median. We limit projections of the forest-fire area to 2050 acknowledging the greater uncertainty in vegetation dynamics, human behavior, and climate trajectories beyond mid-century. Given the wide range of uncertainty in the fire-fuel feedbacks, we present several forms and strengths of fire-fuel feedbacks as guided by the ecological literature that accounts for (1) post-fire tree regeneration failure, (2) the form and strength of fuel limitations imposed by recent fire history, and (3) the modulation of the longevity of fuel limitations during drought[18,22–24].

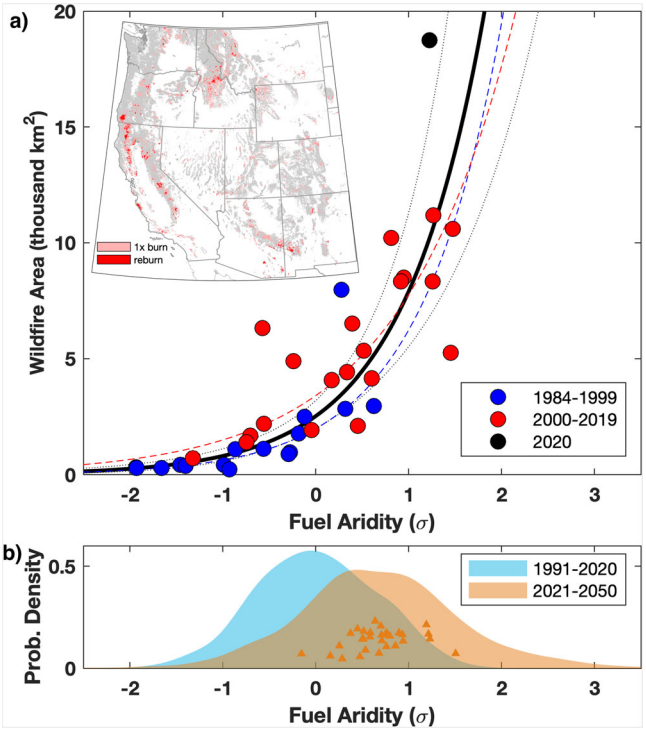

Fig. 1 Nonlinear climate–fire relationships in western US forests. a Interannual relationship between fuel aridity (F) over forested lands vs. annual forest-fire area for the western US. Curves represent regression for the period 1984–2020 (black, dotted shows 95th percentile confidence interval), 1984–1999 (dashed blue), and 2000–2020 (dashed red). Inset map shows forested land burned once (pink) and more than once (red) during 1984–2020. Forested land not burned during 1984–2020 is shown in gray. **b** Probability distribution of F pooled from 30 climate models for 1991–2020 (teal) and 2021–2050 (orange, triangles show the change in mean F for each model).

Results

To project future fire, we first build a model of climate–fire relationships for the observational period and evaluate the model's skill. There is a positive interannual correlation ($r^2 = 0.80$) between F and the logarithm of western US forest-fire area during the modern satellite observational record (1984–2020; Fig. 1a and Supplementary Table 1). These extend the results of previous studies that found strong relationships between burned area and aridity in forested regions of the western US[3,25–27]. Notably, the nonlinear response of forest-fire area to F, suggests that each incremental increase in F leads to a greater response in forest-fire area than prior increases. The 1.0 σ increase in mean F from 1984–1999 to 2000–2020 coincided with a four-fold increase in the upper quartile of annual forest-fire area totals (Fig. 2a).

Cross-validation of the models over the observational period was performed to evaluate non-stationarity in relationships that may arise through exogenous factors and the applicability of empirical models to future conditions. Models built using various subsets of data (1984–2020, 1984–1999, 2000–2020) yield statistically indistinguishable regression parameters (e.g., Fig. 1a).

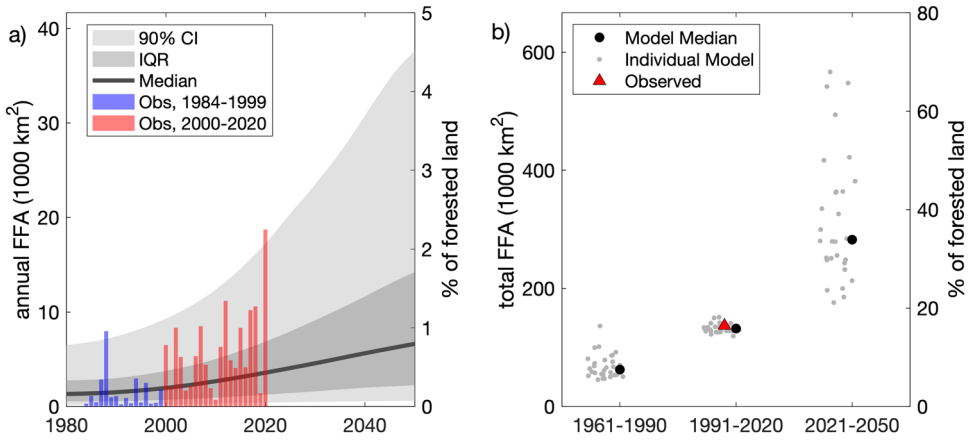

Fig. 2 Modeled changes in the forest-fire area using the static model. a Time series of median, interquartile range, and 5-95% range of annual forest-fire area (FFA) simulated from climate models and the static climate–fire model (historical forcing pre-2015; SSP2-45 forcing 2015–2050). Modeled results show the model median of the statistics calculated using a 21-year centered moving window. Colored bars are observations. **b** Cumulative 30-yr forest-fire area for three time periods showing individual climate models (gray dots) and the 30-model median (large black dots). The observed forest-fire area during 1991–2020 is indicated by the red triangle.

Similarly, models trained on the first portion of the dataset were as skillful in predicting the forest-fire area in the second portion of the dataset (Supplementary Table 2). Results of this cross-validation exercise suggest that changes in fuel extent or other changes in human–environment factors during 1984–2020 did not significantly affect macroscale climate–fire relationships. Further, this cross-validation also suggests that such models can provide near-term predictive utility[27].

Climate models project robust anthropogenic increases in fuel aridity for the next 30 years (Fig. 1b). Averaged across projections made by 30 climate models, F increases by 0.66 $\boldsymbol{\sigma}$ for 2021–2050 compared to 1991–2020 (+0.45 to +0.80 $\boldsymbol{\sigma}$ interquartile range of CMIP6 models), primarily because of warming-induced increases in evaporative demand.

Assuming no changes in fuel extent, our static model yields a doubling (30-model median increase of 107%) in the mean annual forest-fire area during 2021–2050 compared to that observed during 1991–2020 (Fig. 2b)—with the 2021–2050 cumulative forest-fire area equivalent to ~35% of contemporary forested area. While there is substantial intermodel variability, climate projections made by 26 of 30 models lead to at least a 50% increase in forest-fire area (Fig. 2b). We additionally show a two-fold increase in the interquartile range in the annual forest-fire area and a three-fold increase in the probability of years exceeding the record-breaking 2020 season (Fig. 3c, d). However, years with quiescent fire activity are also projected to remain semi-regular occurrences; approximately one-third of the years between 2021 and 2050 are projected to have less forest-fire area than the observed median annual forest-fire area during 1991–2020 (Fig. 3e).

Our dynamic models suggest that the area ineligible to burn because of past fire L declined over the twentieth century (Fig. 4), supporting the well-documented fire deficit and increase in forest biomass across western US forests from pre-colonization baselines due to fire suppression[28]. This decrease in L has heightened the sensitivity of the contemporary forest-fire area to F. Yet, our models suggest that the recent increase in the forest-fire area has reversed the twentieth-century decline in L.

The dynamic models that include a wide range of feedback strengths and durations only modestly reduce the magnitude of the projected increase in forest-fire area (Fig. 3a, b). Dynamic models with weak and moderate fire-fuel feedbacks show increases in the mean annual forest-fire area of 82–90% and 63–75%, respectively, compared to the 107% increase projected by the static model. The dynamic model with the strongest fire-fuel negative feedback yields a 46% increase in the forest-fire area during 2021–2050 compared to 1991–2020 observations. Projected increases in forest-fire area facilitate increased L (Fig. 4), increasingly limiting the total forested area eligible to burn[21,24]. Dynamic models also show an increase in year-to-year variability in the forest-fire area and an increase in the probability of years exceeding the 2020 fire season (Fig. 3b, c), albeit with smaller changes than projected by the static model. Finally, the relative effects of dynamic fire-vegetation feedbacks on future fire statistics are relatively insensitive to choices in the form of the feedbacks, parameter values, and the index used to measure aridity F (e.g., CWD). For example, a formulation of L that assumes a weak fire-vegetation feedback results in 14–19% reductions in the future forest-fire area relative to the static model's projection across a range of alternative model parameterizations and inputs (Supplementary Table 3).

Discussion

Our findings suggest that the continued increase of western US forest-fire area due to drying fuels will only be moderately allayed by the eventual constraints on fuel extent and biomass from fire-fuel feedbacks. Even the strongest feedbacks in our models yield significant increases in forest-fire area, probability of extreme fire years, and year-to-year variability in forest-fire area. The projected increase in forest-fire area materializes from thermodynamic responses to anthropogenic climate change[1,27] and the exponential response of forest-fire area to fuel aridity in this contemporary human–environment system. Larger increases in the forest-fire area were found with indices of atmospheric aridity F that do not explicitly include precipitation (e.g., VPD; Supplementary Figs. 1 and 2).

Our study focuses on the aggregate of the forest-fire area in the western US given the robust and dominant relationship between aggregate area burned and climate, and because the leading pattern of variability in fire-season aridity spans the entire western US (Supplementary Fig. 3). Coupled fire-vegetation models with greater granularity may provide richer information by incorporating complex feedback processes[21,24,29]. However, these models are computationally expensive to run for continental domains. Likewise, while we evaluate the strength and longevity of these fire-fuel feedbacks, fire regime characteristics can also be shaped by other disturbance agents leading up to and

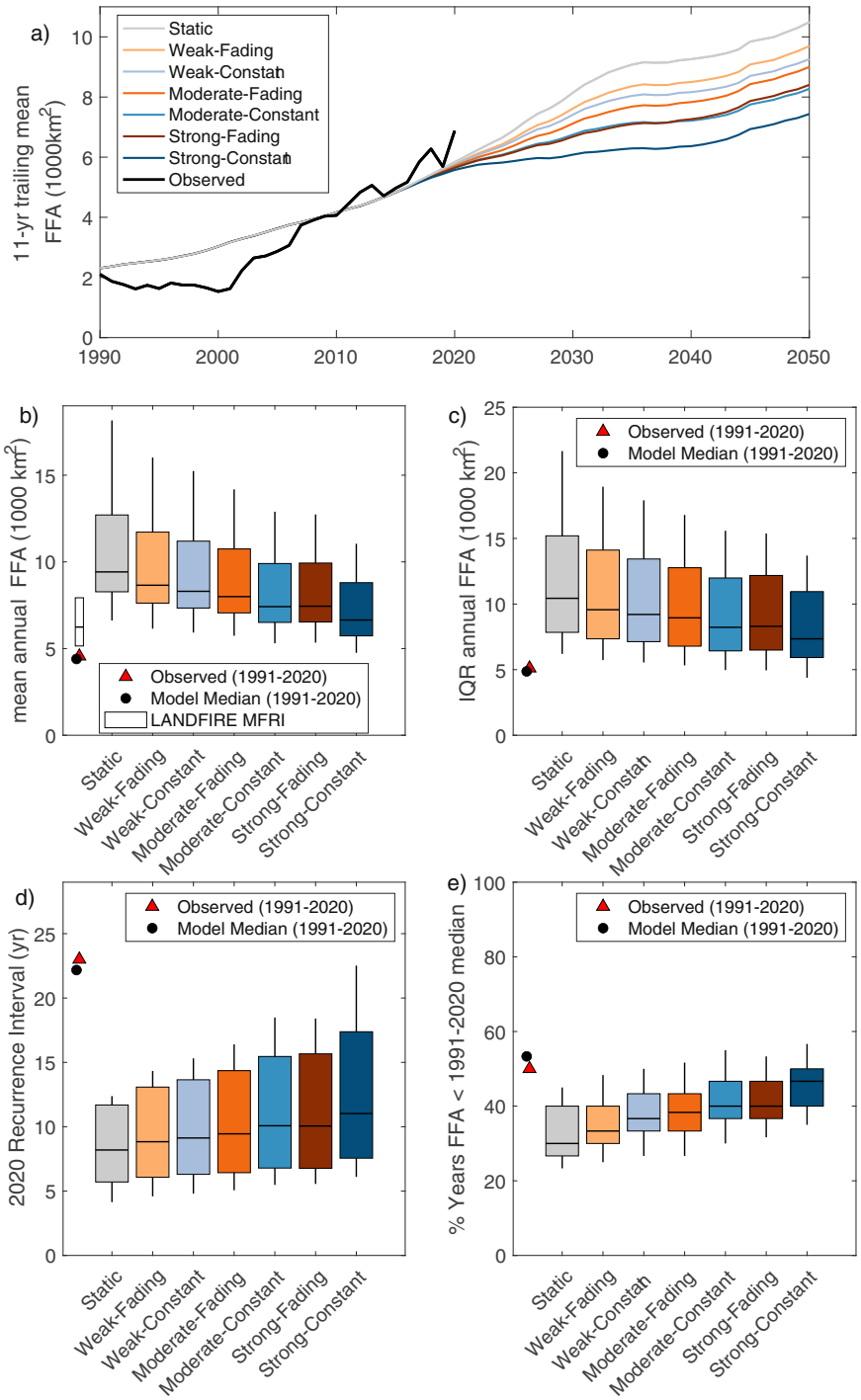

Fig. 3 Forest-fire area (FFA) projections (2021–2050) using static and dynamic models. Shown are (**a**) time series of trailing 11-year moving average forest-fire area, **b** average annual forest-fire area, **c** interquartile range, median and the 10th and 90th percentile for the average annual burned area, **d** recurrence interval of the forest-fire area exceeding the 2020 fire season, and (**e**) percent of years with a forest-fire area less than the 1991–2020 observed median. **a** Results for the multi-model median. Boxplots show the median, interquartile range, and 10–90th percentiles from climate models. The observed and modeled forest-fire area-averaged over the 1991–2020 period are shown by the red triangle and black dot, respectively. Estimated ranges in the annual forest-fire area corresponding to pre-European colonization are shown by the white bar in (**b**). Fire model descriptions are provided in Supplementary Table 2.

following fire events, including insects, drought mortality, windthrow, invasive annual grasses, or anthropogenic disturbances such as harvest. While each disturbance agent can have sizeable impacts on forest mortality[30], their interactions with fire are mixed and context-dependent[31] confounding a credible way of incorporating them herein. We note land area in L is not immune to fire; rather, such lands in post-fire successional trajectories may support grassland and shrubland fire that are not accounted for here. Relatively larger increases in the forested-fire area due to anthropogenic climate change are postulated in mesic flammability-limited forest systems than in drier forest systems[16,32].

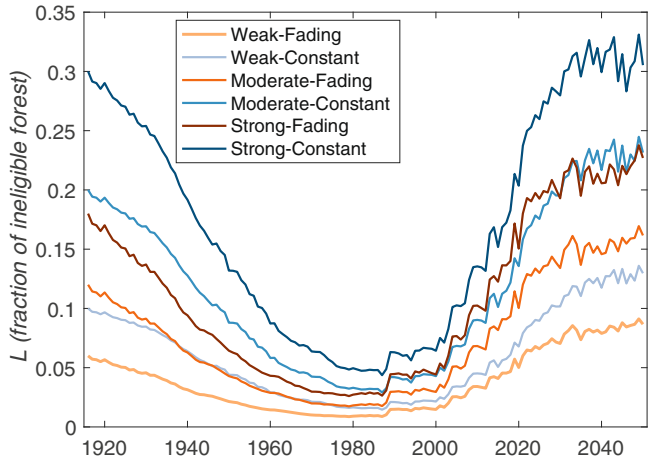

Fig. 4 Modeled fraction of forested land (*L*) ineligible to support forested burned area using various dynamic models. Forest-fire area aggregated over the western US is derived from the estimated forest-fire area from 1916–1983[25] and MTBS/MODIS records from 1984 to 2020. For 2021–2050, we show the median *L* from the 30 climate models.

Lastly, our focus herein is on the forest-fire area; changes in area burned in non-forested lands may differ markedly from those presented here[16]. Anthropogenic modification of fire regimes, including fire suppression, has increased the proportion of western US forests available to burn, particularly at higher intensity, over the twentieth century. Recent repeat forest fires have constrained fire growth and reduced fire severity[33–35], yet macroscale fuel constraints have not yet become evident at the scale of the western US forest area. These feedbacks may become increasingly relevant with increased fire, but the timing, magnitude, and efficacy of such feedbacks are highly uncertain and warrant further study. That being said, our results suggest feedbacks between fire and fuel alone will very likely be insufficient to reverse the rapid and ongoing increases in annual western US forest-fire area in the coming decades. Notably, however, the binary definition of fire area does not capture the local variation in fire intensity, and some portion of increasing fire area will undoubtedly be the lower-intensity, ecologically beneficial fire that restores fire-adapted, dry forest ecosystems.

Western North American forests evolved with fire, however, such fire was characteristically far different than the contemporary period and included thousands of cultural fires set by Indigenous people that burned over days to months[36]. Continued increases in the recent trend of megafires that are driving greater forest-fire area have negative socio-ecological consequences including fatalities, destruction of infrastructure[37], and ecosystem impacts such as widespread tree regeneration failure[38]. Absent broad mitigation and adaptation, losses will increase, highlighting the need for strategies to ameliorate the trajectory of escalating fire impacts[39]. In addition to reducing fossil fuel emissions to slow the impact of increasing aridity, our dynamic models complement the substantial body of literature showing that locally appropriate land management strategies designed to intentionally increase *L* may also slow increases in negative fire impacts[40]. Strategies demonstrated to be effective in increasing *L* include mechanical fuel reduction and expanding the use of prescribed fire and managed wildfire, particularly when conditions are conducive (e.g., *F* is relatively low) during quiescent fire seasons, which we show will continue to occur despite climate change. While the forest-fire area was more than an order of magnitude than the forested area treated with prescribed fire in the contemporary record[41], scaling up the use of prescribed fire may assist in curtailing negative fire effects through increased *L*. However, further analyses are needed to evaluate potential changes in windows of opportunity for using prescribed fire subject to biophysical (e.g., fuels, weather) and logistical constraints.

It appears unavoidable that absent a massive intervention to modify the intensity and mitigate negative impacts, the western US forest-fire area will continue to increase in the coming decades. Recent years indicate this will likely occur primarily through the occurrence of problematic megafires, even as fuel-limitation feedbacks begin to slow this increase. It is also critical to recognize that not all fire has negative outcomes[42], and mitigation and adaptation strategies can alter the outcomes of increasing fire. Dynamic models with stronger feedbacks yielded forest-fire area similar to estimates from the pre-colonization era—levels of the forest-fire area under which modern forest ecosystems evolved. As most area burned is low or moderate-severity fire, such increases in fire activity could ultimately facilitate ecosystem restoration, but mitigating fire disasters will be crucial. Managers and policymakers can carefully consider where management actions are most beneficial, the challenges of implementing such actions, and how these approaches scale geographically to meaningfully alter widespread outcomes[43].

Methods

Data sets. Monthly climate data of maximum and minimum temperature, dew-point temperature, and precipitation at a 1/24th degree horizontal resolution from 1950 to 2020 was acquired from the Parameterized Regression on Independent Slopes Model (PRISM)[44]. Monthly surface downward shortwave radiation and 10-m wind speeds at a 0.25-degree horizontal resolution were acquired from ERA-5[45] for the same period and bilinearly interpolated to the PRISM grid. Monthly data for the same variables from a single ensemble member from each of 30 climate models participating in the Sixth Coupled Model Intercomparison Project (CMIP6) were acquired from the historical climate experiment for 1950–2014 and from the SSP2-45 experiment for 2015–2050 and interpolated to a common 1.0-degree horizontal resolution grid (Supplementary Table 4).

Following Abatzoglou and Williams, we calculated three proxies of aridity using monthly climate data: mean vapor pressure deficit (VPD), Penman-Monteith reference evapotranspiration (ETo), and climatic water deficit (CWD[46], defined as ETo minus actual evapotranspiration[3]). We modified ETo to account for potential reduced stomatal conductance due to increasing atmospheric carbon dioxide, which reduces surface resistance to evapotranspiration. We made this modification following the method of Yang et al.[47]. Importantly, the effect of CO_2 on surface resistance at the scale of the western US is highly uncertain and this method derives the strength of this effect from earth system models. Each index was calculated as follows. At each grid cell, we calculated mean Mar–Sep VPD, the sum of Mar–Sep ETo, and Jan-Dec CWD; each of these time series was standardized to the 1991–2020 baseline using z-score transformations to create a fuel aridity index *f* for each grid cell. The regionally averaged fuel aridity index *F* was calculated by first taking the average of *f* over grid cells that have a majority of land classified as forest or woodland in the LANDFIRE environmental site potential product[48]. We then re-standardized *F* relative to the 1991–2020 reference period and applied equidistant quantile mapping[49] to each model. The latter ensures that the distributions of modeled *Z* match those of observed *Z* for the 1991–2020 period while preserving changes in *Z* from this reference period. Herein we used CWD for *F* because it presents a more balanced view of precipitation and atmospheric demand than VPD or ETo alone, exhibits strong links to the forest-fire area over the observational record, and has more conservative increases in fire under future climate (Supplementary Fig. 2). The variance explained in forest-fire area when defining *F* as VPD, ETo, and detrended CWD is presented in Supplementary Table 1. We note that our approach does not explicitly incorporate daily meteorology such as the number of dry days or critical fire-weather patterns[10] beyond that already included in *F*.

Burned area data from wildland fires were acquired from Monitoring Trends in Burn Severity (MTBS) during 1984–2018[50] and from the version 6 MODIS burned area dataset during 2001–2020[51]. The forested burned area was aggregated by lands classified as forest or woodland[48]. MTBS includes primarily fires ≥404 ha that comprises>95% of burned area in the region[52]. We further excluded areas in the unburned-to-low burn severity class[53] as well as fires classified as prescribed burns in MTBS. Further, we did not include forested area treated by prescribed fire as a contemporary area for prescribed fire is more than an order of magnitude less than that of forest-fire area[41]. Forest-fire area estimates for 2019–2020 were obtained using adjusted burned areas from MODIS based on a linear model that relates MODIS and to the MTBS forest-fire area time series during the overlapping 2001–2018 period[26].

Experimental design. We focus on macroscale climate–fire models operating at the scale of the entire western US forested area. While there is value in spatially refined models, efforts to parameterize empirical relationships at localized scales can be limited by the stochastic nature of ignitions and fire weather—particularly in locations with long fire return intervals with zero-inflated distributions of annual burned area. Strong interannual relationships between fuel aridity and strain on national fire suppression resources shared across the region highlight the implicit value in considering larger spatial scales[54]. The macroscale approach is further justified because the leading mode of variability in fuel aridity across forested land is a commonly signed regionwide pattern that is strongly correlated ($r^2 = 0.79$) to the logarithm of forest-fire area (Supplementary Fig. 3).

Static model. Following previous empirical models of annual forest-fire area[3,25], we first consider a static model of western US annual forest-fire area (FFA) based on F (fuel aridity) of the form:

$$\log(\mathrm{FFA}(t)) = \alpha_s + \beta_s F(t) + \varepsilon, \quad (1)$$

where t is the year, α_s and β_s, are regression coefficients, and ε represents an error term. We use annual CWD for F as it accounts for precipitation and atmospheric demand, exhibits strong interannual relationships with FFA, and provide more conservative estimates of projected changes in aridity and thus area burned than other aridity metrics such as VPD[3,7,12]. The error term ε is drawn from the population of the log-residual of observed minus modeled FFA. This error term represents variability not captured in the FFA–F relationship (e.g., extreme fire-weather conditions, human ignitions) that is important for the full distribution of FFA.

Dynamic models. The contemporary climate–fire relationship in Eq. 1 should persist with increased F until increased burned area and severity cause fuel limitations[15]. Fire-fuel feedbacks that alter the climate–fire relationship primarily occur through temporary reduction of fine fuels; such feedbacks can reduce the burning potential for approximately three decades post-fire[38,55]. Further, longer-lived reductions in the forest-fire area can occur when forests do not recover from fire and instead transition to non-forest vegetation that can still carry fire. However, constraints on the area burned imposed by fire-fuel feedbacks are weakened by concurrent drought, which allows the fire to propagate across sparser fuels, and can markedly shorten the window of reduced burning[18].

We incorporate these effects through a term L, which represents the fraction of contemporary forested land that is incapable of carrying fire in a predominately forested environment in a given year, in a dynamic model of the form:

$$\log\left(\frac{\mathrm{FFA}}{1 - L(t)}\right) = \alpha_d + \beta_d F(t) + \varepsilon, \quad (2)$$

where the response of log(FFA) to fuel aridity reduces as a function of L. We present various potential forms and strengths of fire-fuel feedbacks in L that are guided by the ecological literature and account for post-fire tree regeneration failure, fuel limitations imposed by recent fire history, and waning of fuel limitations during drought[18,22–24]. L is influenced by semi-permanent limitations due to failure of post-fire forest regeneration (L_{rf}), and temporary limitations due to recent fire history (L_f):

$$L(t) = L_{rf}(t) + L_f(t). \quad (3)$$

Importantly, L is poorly constrained and likely varies in geographically and temporally complex ways[18,34]. For example, L can differ for a fixed fraction of recently burned forest. A relatively small L implies weak feedbacks allowing forests to more easily reburn. A relatively large L implies strong feedbacks, for example, where heterogeneous fire effects create patch mosaics that constrain fire spread even though there is ample fuel. Finally, the age threshold for L may decrease with continued climate change, with some indications that recent fires burned through forests <10 years post-fire.

Post-fire tree regeneration failure L_{rf}. Summer soil moisture deficits in the years post-fire may reduce tree regeneration[19,38]. Absent reforestation, the failure of post-fire forest regeneration represents a semi-permanent reduction in forested land available to burn. Post-fire regeneration is strongly dependent on site-specific thresholds in growing-season moisture requirements[23,56], burn severity and distance to the seed source, as well as species composition. We estimate the fraction (ρ) of forest that is permanently lost due to the failure of post-fire regeneration using the mean fuel aridity over the 3-year post-fire period (F_{3y}) because protracted drought stress in the years immediately following fire has been shown to limit the establishment of some tree species[57]. This is done using a simple linear transform:

$$\rho(t) = \begin{cases} 0, F_{3y} < 1 \\ \mu(F_{3y} - 1), 1 < F_{3y} \le 2 \\ \mu, F_{3y} > 2 \end{cases}, \quad (4)$$

where μ is set at 0.1 (Eq. 4 is plotted in Supplementary Fig. 4a). Hence, the fraction of forested land that is semi-permanently ineligible to carry forest fire because previously burned forest did not regenerate as forest (L_{rf}) is the cumulative sum of the product of annual FFA and ρ since 1984:

$$L_{rf}(t) = \sum_{i=1984}^{t} \frac{\rho(t)\mathrm{FFA}(t)}{T}, \quad (5)$$

where T refers to the contemporary area of forested land[48]. Note that Eq. 4 and μ can be modified to account for the diversity of species-specific responses at local-to-regional scales given the acknowledgement that some species are more resilient than others and local plant water stress alters regeneration probabilities[58,59]. Overall, L_{rf} as parameterized here resulted in values approaching L_{rf} ~0.01 by 2050, suggesting that the inability of trees to regenerate post-fire is a minor contributor to fire-fuel feedbacks through mid-century. Modifications to the parameters in Eq. 4 resulted in only minor differences in projected FFA (Supplementary Table 3).

Temporary fire-fuel feedbacks L_f. Most studies in forested environments show strong fire-fuel feedbacks in the first 5–10 years post-fire[55,60]. This temporary fire-fuel feedback, which we refer to here as L_f, tends to wane after 10 years[60], with the longevity τ of the fire-fuel feedbacks varying geographically, from as short as ~15 years in warmer sites in the southwest to over ~30 years in cold mesic systems in the northern Rockies[18]. Herein, we use a baseline $\tau = 30$ years, which results in a conservative estimate of future area burned.

We consider two forms for how L_f incorporates information on annual fire histories over the previous τ years: a constant feedback and a fading feedback. These forms of L_f are defined below in Eqs. 6 and 7 and plotted in Supplementary Fig. 4c.

In the case of the constant feedback, the effect of burned area on L_f remains constant over the τ years following fire. At the scale of the whole western US forested area, the constant form, therefore, assumes that the transient limitation is simply proportional to the total FFA over the preceding τ years:

$$L_f(t) = \gamma \sum_{i=-\tau}^{-1} \frac{\mathrm{FFA}(i)}{T}. \quad (6)$$

In Eq. 6, parameter γ represents the strength of the feedback, described in more depth below.

The fading feedback form of L_f more heavily weights the contribution from recent FFA compared to older FFA. At the scale of the whole western US forested area, this form applies constant weight to FFA in the five most recent years given strong fire-fuel feedbacks of recent fires, and increasingly reduces the contributions from prior years based on a sinusoid function:

$$L_f(t) = \gamma \frac{\sum_{i=-5}^{-1} \mathrm{FFA}(i) + \sum_{i=-\tau}^{-6} \mathrm{FFA}(i) * \left[1 - \cos\frac{\pi(-i-5)}{\tau-5}\right]/2}{T}. \quad (7)$$

Given the uncertainty in the efficacy of the fire-fuel feedback, we present results using both the constant and fading formulations for the temporary fire-fuel feedbacks.

We additionally considered three different fuel-limitation strengths γ in Eqs. 6 and 7 to account for direct and indirect potential effects of past fires: $\gamma = 0.5$, referred to as weak; $\gamma = 1$, referred to as moderate; and $\gamma = 1.5$, referred to as strong. For the weak ($\gamma = 0.5$) fuel-limitation case using the constant feedback model, the fractional forested area ineligible to burn is only half of the total area burned in the past 30 years, indicating that half of recent burned areas can reburn. For the strong-constant fuel-limitation case, the forested area ineligible to burn post-fire exceeds the total recent burned area by 50%. An example of a strong fuel limitation is a burn mosaic with reduced connectivity that constrains the ability of subsequent fire spread into the adjacent forest that did not burn in the previous τ years. We considered higher values of γ, but these yielded degraded cross-validation skills when modeling the historical period (Supplementary Table 2).

Longevity of fire-fuel feedbacks during drought. Finally, some temporary fuel limitations can be overcome during extreme fire-weather conditions and during periods of drought. For example, while reduced fuel loads in a post-fire landscape serve as an effective barrier for fire propagation under moderate fuel aridity, the fire spread probability increases with increasing F[34]. Studies have found that the longevity of fire-fuel feedbacks was a third shorter during periods of extreme drought than in periods without drought stress[18,34]. For example, there is evidence of short-interval (<20 years) stand-replacing fires in systems with 100–300 year mean fire return intervals—suggesting that such systems can carry fire under warmer and drier fire-weather conditions[20,33,61]. We incorporate this effect by making the longevity parameter τ a function of contemporaneous $F(t)$, where τ reduces linearly from 30 years toward 20 years as fuel aridity increases from 1991 to 2020 mean ($F = 0$) to two standard deviations above the mean ($F \ge 2$):

$$\tau = \begin{cases} 30, F < 0 \\ 30 - 5F, 0 < F \le 2 \\ 20, F \ge 2 \end{cases}. \quad (8)$$

The form of τ is plotted in Supplementary Fig. 4b. The resultant weighting of L_f in the fading model using the end-members of τ is displayed in Supplementary Fig. 4d.

Running the model. Dynamic models were run over the twentieth century (1916–1983) using proximal estimates of FFA[25] calibrated to the observational record[62]. Nominally, LANDFIRE's gridded mean fire return interval (MFRI), an estimate of the average number of years between fires, was used to approximate a baseline FFA prior to 1916. This was used to initialize the model and serve as a reference point for projected FFA. We calculated three estimates based on the reported range for each categorical MFRI across the landscape (e.g., 11–15 years): a midpoint MFRI (e.g., 13 years), as well as the lower (e.g., 11 years) and upper bounds (e.g., 15 years) of MFRI estimates. We recognize that MFRI estimates are prone to uncertainty[63], and that such estimates reflect conditions prior to European colonization which likely differ from those in the late 1800s and early 1900s[28,64]. However, the LANDFIRE MFRI represents the only wall-to-wall dataset of estimated fire regime parameters relevant to our study here and provide a range of likely estimates.

FFA estimates prior to the satellite era are prone to uncertainties[25,65]. However, initial conditions do not influence model sensitivity over the 1984–2020 period. Rather, FFA estimates serve to highlight that our formulation of L captures the increase in fuel extent in the second half of the twentieth century due to the fire deficit associated with forest management practices[5,28]. Finally, no significant difference in climate–fire correlations over the observational record were seen using dynamic models compared to the static models, suggesting that the influence of changes in L in recent decades has had little impact on recent fire-climate relationships—either because L has not changed significantly or that $L \ll 1$ over the observational period (1984–2020). Our dynamic models suggest that suppressed L during the observational period has heightened FFA sensitivity to F.

Static and dynamic models were applied to the climate output of each CMIP6 model for the period 1950–2020 using L calculated from observations prior to 1950 and model-derived thereafter. For the 2021–2050 period, we used the observed FFA record through 2020 in calculating L and used model-derived FFA thereafter. Both the static and dynamic models implicitly include human and management effects in the regression parameters, and we assume these factors are time-invariant for future projections. Further, for each climate model run, we used a Monte-Carlo resampling procedure ($n = 1000$) that randomizes ε from the observed residual population therein creating 1000 replicates of modeled FFA for each climate model. Herein, we report statistics for the median of the Monte-Carlo simulations for each climate model.

In both static and dynamic models, we limit the area that can burn in a single year. The maximum FFA in the static model is defined by the estimated 100-yr return period FFA for the observational period using extreme value analysis. This works out to be 7.5% of the total forested land T—nearly four times that burned in 2020. For the dynamic models, the maximum forest that is allowed to burn in any year is 7.5% of the forested area that is eligible to burn: i.e., 7.5% of $(1 - L)*T$. We acknowledge that this limit is not well quantified physically but is implemented to constrain the exponential FFA–F relationships used herein. In practice, such limits occur in ~1% of model years for 2021–2050. Similar quantitative results were seen by capping $F \leq 3$, which implies a saturation effect of F on FFA. Finally, while we ran the model at the aggregated scale of western US forests, the model may conceptually be run at subregional scales. We note that the strength of fire-feedbacks, climate–fire relationships, as well as model parameterizations will likely vary on subregional scales.

Statistical information. Model cross-validation was performed to assess the skill of the models. Models using Eqs. 1 and 2 were built using training data during 1984–2000 and validated for 2001–2020. We evaluated skill by three metrics: model bias as the ratio of total modeled FFA to total observed FFA; the coefficient of efficiency (CE) as a measure of accuracy relative to a null model; and the correlation coefficient between modeled and observed log(FFA). Note that measures of bias and CE were calculated using non-log transformed data.

We assessed the statistical significance of cross-validation skill by resampling the residual term ε in Eqs. 1 and 2. This involved developing and testing 1000 iterations of the model subject to a random sampling of ε. We deem a model to have significant skill when >95% of the iterations had bias CE > 0, >95% of the iterations had $r > 0$, and the inner 95% of the simulations included a bias of 0.

Supplementary Table 2 shows that the static model and many of the dynamic models have significant cross-validated skills. However, skill decreased in the dynamic models as the feedback strength increases. While the weak dynamic feedback models had similar cross-validation skill as the static model, dynamic models with very strong feedbacks ($\gamma \geq 2$) had sizeable underpredictions in FFA by up to 46% for the validation period. Hence, we excluded such parameters from the further analysis given that such results were incongruent with the observational record.

Three statistical metrics of annual variability of FFA were calculated for both static and dynamic models. First, we used generalized extreme value theory to estimate recurrence intervals for FFA greater than equal to that of the 2020 fire season. Second, we calculated the interquartile range (IQR) in modeled FFA to examine changing interannual variability. Lastly, we examined the percent of years with modeled FFA below the 1991–2020 observed median as a measure of quiescent fire years. Calculations were performed separately for each climate model for 1991–2020 and 2021–2050.

Data availability

Observed gridded climate data sets are publicly available from the PRISM Climate Group, Oregon State University (http://prism.oregonstate.edu) and ERA-5 (https://cds.climate.copernicus.eu/), while CMIP6 (Supplementary Table 4) model output is available through the Earth System Grid Foundation (ESGF). Gridded burned area data are available through the Monitoring Trends in Burn Severity Program (http://mtbs.gov) and MODIS global burned area product MCD64A1 (https://modis-fire.umd.edu/ba.html). Summarized time series of observed annual F and FFA through 2020 as well as summarized annual modeled data from 30 different CMIP6 projections are provided on Dryad (https://datadryad.org/stash/share/yxGFk_OS2FyR8C1nBaExc9uWakmbtndhmq8xiEkoInM).

Code availability

Software for running the various models is available at https://github.com/abatz/firemodel.

Received: 16 July 2021; Accepted: 6 October 2021;
Published online: 02 November 2021

References

1. Westerling, A. Increasing western US forest wildfire activity: sensitivity to changes in the timing of spring. *Philos. Trans. R. Soc. B Biol. Sci.* **371**, 20150178 (2016).
2. Higuera, P. E. & Abatzoglou, J. T. Record-setting climate enabled the extraordinary 2020 fire season in the western United States. *Glob. Chang. Biol.* **27**, 1–2 (2021).
3. Abatzoglou, J. T. & Williams, A. P. Impact of anthropogenic climate change on wildfire across western US forests. *Proc. Natl. Acad. Sci. USA* **113**, 11770–11775 (2016).
4. North, M. P. et al. Reform forest fire management. *Science* **349**, 1280–1281 (2015).
5. Parks, S. A. et al. Wildland fire deficit and surplus in the western United States, 1984–2012. *Ecosphere* **6**, 1–13 (2015).
6. Hagmann, R. K. et al. Evidence for widespread changes in the structure, composition, and fire regimes of western North American forests. *Ecol. Appl.* https://doi.org/10.1002/eap.2431 (2021).
7. Abatzoglou, J. T., Williams, A. P., Boschetti, L., Zubkova, M. & Kolden, C. A. Global patterns of interannual climate-fire relationships. *Glob. Chang. Biol.* **24**, 5164–5175 (2018).
8. Jolly, W. et al. Climate-induced variations in global wildfire danger from 1979 to 2013. *Nat. Commun.* **6**, 7537 (2015).
9. Flannigan, M. et al. Global wildland fire season severity in the 21st century. *For. Ecol. Manage.* **294**, 54–61 (2013).
10. Holden, Z. A. et al. Decreasing fire season precipitation increased recent western US forest wildfire activity. *Proc. Natl. Acad. Sci. USA* **115**, E8349–E8357 (2018).
11. Stavros, E. N. N., Abatzoglou, J. T. J. T., McKenzie, D. & Larkin, N. K. N. K. Regional projections of the likelihood of very large wildland fires under a changing climate in the contiguous Western United States. *Clim. Change* **126**, 455–468 (2014).
12. Brey, S. J., Barnes, E. A., Pierce, J. R., Swann, A. L. S. & Fischer, E. V. Past variance and future projections of the environmental conditions driving western U.S. summertime wildfire burn area. *Earth's Future* **9**, e2020EF001645 (2021).
13. Abatzoglou, J. T., Williams, A. P. & Barbero, R. Global emergence of anthropogenic climate change in fire weather indices. *Geophys. Res. Lett.* **46**, 326–336 (2019).
14. Goss, M. et al. Climate change is increasing the risk of extreme autumn wildfire conditions across California. *Environ. Res. Lett.* **15**, 094016(2020).
15. McKenzie, D. & Littell, J. S. Climate change and the eco-hydrology of fire: will area burned increase in a warming western U.S.? *Ecol. Appl.* **27**, 26–36 (2017).
16. Littell, J. S., McKenzie, D., Wan, H. Y. & Cushman, S. A. Climate change and future wildfire in the western United States: an ecological approach to nonstationarity. *Earth's Future* **6**, 1097–1111 (2018).
17. Westerling, A. L., Turner, M. G., Smithwick, E. A. H., Romme, W. H. & Ryan, M. G. Continued warming could transform Greater Yellowstone fire regimes by mid-21st century. *Proc. Natl. Acad. Sci. USA* **108**, 13165–13170 (2011).
18. Parks, S. A., Parisien, M., Miller, C., Holsinger, L. M. & Baggett, L. S. Fine-scale spatial climate variation and drought mediate the likelihood of reburning. *Ecol. Appl.* **28**, 573–586 (2018).
19. Coop, J. D. et al. Wildfire-driven forest conversion in western North American landscapes. *Bioscience* **70**, 659–673 (2020).
20. Turner, M. G., Braziunas, K. H., Hansen, W. D. & Harvey, B. J. Short-interval severe fire erodes the resilience of subalpine lodgepole pine forests. *Proc. Natl. Acad. Sci. USA* **116**, 11319–11328 (2019).
21. Hurteau, M. D., Liang, S., Westerling, A. L. & Wiedinmyer, C. Vegetation-fire feedback reduces projected area burned under climate change. *Sci. Rep.* **9**, 2838 (2019).
22. Parks, S. A., Miller, C., Holsinger, L. M., Baggett, L. S. & Bird, B. J. Wildland fire limits subsequent fire occurrence. *Int. J. Wildl. Fire* **25**, 182–190 (2016).

23. Davis, K. T. et al. Wildfires and climate change push low-elevation forests across a critical climate threshold for tree regeneration. *Proc. Natl. Acad. Sci. USA* **116**, 6193–6198 (2019).
24. Hansen, W. D., Abendroth, D., Rammer, W., Seidl, R. & Turner, M. G. Can wildland fire management alter 21st-century subalpine fire and forests in Grand Teton National Park, Wyoming, USA? *Ecol. Appl.* **30**, e02030 (2020).
25. Littell, J. S., McKenzie, D., Peterson, D. L. & Westerling, A. L. Climate and wildfire area burned in western US ecoprovinces, 1916-2003. *Ecol. Appl.* **19**, 1003–1021 (2009).
26. Williams, A. P. et al. Correlations between components of the water balance and burned area reveal new insights for predicting forest fire area in the southwest United States. *Int. J. Wildl. Fire* **24**, 14–26 (2015).
27. Williams, A. P. et al. Observed impacts of anthropogenic climate change on wildfire in California. *Earth's Future* **7**, 892–910 (2019).
28. Marlon, J. R. et al. Long-term perspective on wildfires in the western USA. *Proc. Natl. Acad. Sci. USA* **109**, E535–E543 (2012).
29. Kennedy, M. C., Bart, R. R., Tague, C. L. & Choate, J. S. Does hot and dry equal more wildfire? Contrasting short- and long-term climate effects on fire in the Sierra Nevada. *CA. Ecosph.* **12**, e03657 (2021).
30. Berner, L. T., Law, B. E., Meddens, A. J. H. & Hicke, J. A. Tree mortality from fires, bark beetles, and timber harvest during a hot and dry decade in the western United States (2003–2012). *Environ. Res. Lett.* **12**, 065005 (2017).
31. Donato, D. C. et al. Post-wildfire logging hinders regeneration and increases fire risk. *Science* **311**, 352 LP–352352 (2006).
32. Hanan, E. J. et al. How climate change and fire exclusion drive wildfire regimes at actionable scales. *Environ. Res. Lett.* **16**, 024051 (2020).
33. Harvey, B. J., Donato, D. & Turner, M. G. Burn me twice, shame on who? Interactions between successive forest fires across a temperate mountain region. *Ecology* **97**, 2272–2282 (2016).
34. Parks, S. A., Holsinger, L. M., Miller, C. & Nelson, C. R. Wildland fire as a self-regulating mechanism: the role of previous burns and weather in limiting fire progression. *Ecol. Appl.* **25**, 1478–1492 (2015).
35. Parks, S. A., Miller, C., Nelson, C. R. & Holden, Z. A. Previous fires moderate burn severity of subsequent wildland fires in two large western US wilderness areas. *Ecosystems* **17**, 29–42 (2014).
36. Stewart, O. C. *Forgotten Fires: Native Americans and the Transient Wilderness* (University of Oklahoma Press, 2002).
37. Bowman, D. M. J. S. et al. Human exposure and sensitivity to globally extreme wildfire events. *Nat. Ecol. Evol.* **1**, 58 (2017).
38. Stevens-Rumann, C. S. et al. Evidence for declining forest resilience to wildfires under climate change. *Ecol. Lett.* **21**, 243–252 (2018).
39. Schoennagel, T. et al. Adapt to more wildfire in western North American forests as climate changes. *Proc. Natl. Acad. Sci. USA* **114**, 4582–4590 (2017).
40. Prichard, S. J. et al. Adapting western North American forests to climate change and wildfires: ten common questions. *Ecol. Appl.* e02433 (2021).
41. Kolden, C. A. We're not doing enough prescribed fire in the Western United States to mitigate wildfire risk. *Fire* **2**, 30 (2019).
42. Kolden, C. Wildfires: count lives and homes, not hectares burnt. *Nature* **586**, 9 (2020).
43. Hessburg, P. F., Prichard, S. J., Hagmann, R. K., Povak, N. A. & Lake, F. K. Wildfire and climate change adaptation of western North American forests: a case for intentional management. *Ecol. Appl.* https://doi.org/10.1002/eap.2432 (2021).
44. Daly, C. et al. Physiographically sensitive mapping of climatological temperature and precipitation across the conterminous United States. *Int. J. Climatol.* **28**, 2031–2064 (2008).
45. Hersbach, H. et al. The ERA5 global reanalysis. *Q. J. R. Meteorol. Soc.* **146**, 1999–2049 (2020).
46. Stephenson, N. Actual evapotranspiration and deficit: biologically meaningful correlates of vegetation distribution across spatial scales. *J. Biogeogr.* **25**, 855–870 (1998).
47. Yang, Y., Roderick, M. L., Zhang, S., McVicar, T. R. & Donohue, R. J. Hydrologic implications of vegetation response to elevated CO_2 in climate projections. *Nat. Clim. Chang.* **9**, 44–48 (2019).
48. Rollins, M. G. LANDFIRE: a nationally consistent vegetation, wildland fire, and fuel assessment. *Int. J. Wildl. Fire* **18**, 235–249 (2009).
49. Li, H., Sheffield, J. & Wood, E. F. Bias correction of monthly precipitation and temperature fields from Intergovernmental Panel on Climate Change AR4 models using equidistant quantile matching. *J. Geophys. Res. Atmos.* **115**, D10101 https://doi.org/10.1029/2009JD012882 (2010).
50. Eidenshink, J. C. et al. A project for monitoring trends in burn severity. *Fire Ecol.* **3**, 3–21 (2007).
51. Giglio, L., Boschetti, L., Roy, D. P., Humber, M. L. & Justice, C. O. The Collection 6 MODIS burned area mapping algorithm and product. *Remote Sens. Environ.* **217**, 72–85 (2018).
52. Short, K. A spatial database of wildfires in the United States, 1992-2011. *Earth Syst. Sci. Data* **6**, 1–27 (2014).
53. Kolden, C. A., Smith, A. M. S. & Abatzoglou, J. T. Limitations and utilisation of Monitoring Trends in Burn Severity products for assessing wildfire severity in the USA. *Int. J. Wildl. Fire* **24**, 1023–1028 (2015).
54. Abatzoglou, J. T., Juang, C. S., Williams, A. P., Kolden, C. A. & LeRoy Westerling, A. Increasing synchronous fire danger in forests of the western United States. *Geophys. Res. Lett.* **48**, e2020GL091377 (2020).
55. Prichard, S. J., Stevens-Rumann, C. S. & Hessburg, P. F. Tamm review: shifting global fire regimes: lessons from reburns and research needs. *For. Ecol. Manage.* **396**, 217–233 (2017).
56. Davis, K. T. et al. Fire-catalyzed vegetation shifts in ponderosa pine and Douglas-fir forests of the western United States. *Environ. Res. Lett.* **15**, 1040b8 (2020).
57. Littlefield, C. E., Dobrowski, S. Z., Abatzoglou, J. T., Parks, S. A. & Davis, K. T. A climatic dipole drives short-and long-term patterns of postfire forest recovery in the western United States. *Proc. Natl. Acad. Sci. USA* **117**, 29730–29737 (2020).
58. Hansen, W. D., Braziunas, K. H., Rammer, W., Seidl, R. & Turner, M. G. It takes a few to tango: changing climate and fire regimes can cause regeneration failure of two subalpine conifers. *Ecology* **99**, 966–977 (2018).
59. Stevens-Rumann, C. S. & Morgan, P. Tree regeneration following wildfires in the western US: a review. *Fire Ecol.* **15**, 15 (2019).
60. Ager, A. A. et al. Effects of accelerated wildfire on future fire regimes and implications for the United States federal fire policy. *Ecol. Soc.* **22**, 12–28 (2017).
61. Nelson, K. N., Turner, M. G., Romme, W. H. & Tinker, D. B. Simulated fire behaviour in young, postfire lodgepole pine forests. *Int. J. Wildl. Fire* **26**, 852–865 (2017).
62. Bowman, D. M. J. S. et al. Vegetation fires in the anthropocene. *Nat. Rev. Earth Environ.* **1**, 500–515 (2020).
63. Van de Water, K. M. & Safford, H. D. A summary of fire frequency estimates for California vegetation before Euro-American settlement. *Fire Ecol.* **7**, 26–58 (2011).
64. Savage, M. & Swetnam, T. W. Early 19th-century fire decline following sheep pasturing in a Navajo ponderosa pine forest. *Ecology* **71**, 2374–2378 (1990).
65. Short, K. C. Sources and implications of bias and uncertainty in a century of US wildfire activity data. *Int. J. Wildl. Fire* **24**, 883–891 (2015).

Author contributions

Specific contributions by authors include conceptualization: J.T.A. and D.S.B.; methodology: J.T.A., D.S.B., A.P.W., and W.D.H.; investigation: J.T.A., D.S.B., A.P.W., W.D.H., B.J.H., and C.A.K.; visualization: J.T.A.; writing—original draft: J.T.A. and D.S.B.; writing—review and editing: J.T.A., D.S.B., A.P.W., W.D.H., B.J.H., and C.A.K..

Competing interests

The authors declare no competing interests.

Additional information

Supplementary information The online version contains supplementary material available at https://doi.org/10.1038/s43247-021-00299-0.

Correspondence and requests for materials should be addressed to John T. Abatzoglou.

Peer review information *Communications Earth & Environment* thanks Luke Collins and the other, anonymous, reviewer(s) for their contribution to the peer review of this work. Primary Handling Editor: Clare Davis.

Reprints and permission information is available at http://www.nature.com/reprints

Publisher's note Springer Nature remains neutral with regard to jurisdictional claims in published maps and institutional affiliations.

Open Access This article is licensed under a Creative Commons Attribution 4.0 International License, which permits use, sharing, adaptation, distribution and reproduction in any medium or format, as long as you give appropriate credit to the original author(s) and the source, provide a link to the Creative Commons license, and indicate if changes were made. The images or other third party material in this article are included in the article's Creative Commons license, unless indicated otherwise in a credit line to the material. If material is not included in the article's Creative Commons license and your intended use is not permitted by statutory regulation or exceeds the permitted use, you will need to obtain permission directly from the copyright holder. To view a copy of this license, visit http://creativecommons.org/licenses/by/4.0/.

© The Author(s) 2021